Theoretical Study on Photophysical Properties of Multifunctional Electroluminescent Molecules with Different π-Conjugated Bridges

Lu Yi Zou,[†] Ai Min Ren,*,[†] Ji Kang Feng,*,[†,‡] Yan Ling Liu,[†] Xue Qin Ran,[†] and Chia Chung Sun[†]

State Key Laboratory of Theoretical and Computational Chemistry, Institute of Theoretical Chemistry, Jilin University, Changchun 130023, China, and College of Chemistry, Jilin University, Changchun 130023, China

The photophysics of a series of molecular organic light-emitting diodes (OLEDs) has been studied by theoretical calculation. These molecular OLEDs have been integrated by an electron- and hole-transporting components as well as an emitting components into the donor-π-acceptor (D-π-A) structures: 2-carbazolyl-7-dimesitylboryl-9,9-diethylfluorene (**1**), *trans*-4′-*N*-carbazolyl-4-dimesitylborylstilbene (**2**), and *trans*-2-[(4′-*N*-carbazolyl)styryl]-5-dimesitylborylthiophene (**3**). To reveal the relationship between the structures and properties of these multifunctional electroluminescent materials, the ground- and excited-state geometries were optimized at the B3LYP/6-31G(d), HF/6-31G(d), and CIS/6-31G(d) levels, respectively. The ionization potentials and electron affinities were computed. The mobilities of hole and electron in these compounds were studied computationally based on the Marcus electron transfer theory. The lowest excitation energies (E_g) and the maximum absorption and emission wavelengths of these compounds were calculated by time-dependent density functional theory methods. The solvent effect on the emission spectra of these compounds was considered by a polarizable continuum model. As a result of these calculations, it was concluded that the electron injections of these compounds are much easier than $Mes_2B[p$-4,4′-biphenyl-NPh(1-naphthyl)]$, and the diethylfluorene-based compound has higher electron mobility and better equilibrium properties as compared to the stilbene-based and styrylthiophene-based compounds.

1. Introduction

The development of organic light-emitting diodes (OLEDs) has been progressed tremendously due to their potential applications in many fields.[1−6] Recently, thin multilayer OLEDs have received extensive attention for the potential use in the next-generation full-color flat-panel displays. This includes the applications in car radios, mobile phones, digital cameras, camcorders, personal digital assistants (PDAs), games, notebook personal computers (PCs), etc.[7,8] To simplify the process and reduce the costs of the fabrication of OLED devices, single-layer devices with improved efficiency for light-emission become a hot topic in this filed. It is therefore necessary to design and synthesize multifunctional OLED materials, which are capable of transporting both holes and electrons in addition to functionalizing as efficient emitters, with excellent performance.[9−12] Nowadays, the experimental research on B−N compounds as a sort of multifunctional OLEDs is in full swing,[13−19] and here we investigate the microcosmic mechanism of the luminescent properties to provide some useful information for the experimentalist. In these B−N compounds, the response of organic molecules under the electric field is mainly affected by the polarization of its π-electron. The amount of π-electrons, the delocalization degree, and the property of polarization have direct influence on the energy structure and optoelectronic properties. Also, a discussion on the π-conjugated bridge, which plays an important role in these multifunctional molecules, has been carried out in this paper.

Herein, three molecules, which have the same carbazolyl donor and B(mesityl)$_2$ acceptor group as well as different π-conjugated bridges (Figure 1), have been chosen as the objects. An in-depth interpretation of the optical and electronic properties of these compounds has been presented. The geometrical structure and optical properties of these compounds are given by density functional theory (DFT), ab initio HF and CIS, and time-dependent density functional theory (TD-DFT) methods. The calculated energies are in good agreement with the experimental data. This suggests that the adopted methods and basis set are reasonable.

2. Computational Methods

All of the calculations of the three studied compounds in this work have been performed on the SGI origin 2000 server using the Gaussian03 program package.[20] Geometric and electronic structures of the considered these molecules, as well as their cationic and anionic structures, were investigated making use of DFT. Following each optimization, the vibrational frequencies were calculated and the results showed that all optimized structures are stable geometric structures. The lowest singlet excited states were computed with ab initio CIS/6-31G(d) on the basis of the optimized geometries obtained from HF/6-31G(d) calculations. The theoretical energy gap and experimental band gap have been estimated from the highest-occupied molecular orbital (HOMO)−lowest-unoccupied molecular orbital (LUMO) gaps and the lowest excited energies, respectively. The transition energies were calculated at the ground-state and excited-state geometries using TD-DFT calculations, and the results were compared with the available experimental data. The maximum absorption and emission wavelengths of these

---

* To whom correspondence should be addressed. E-mail: aimin.ren@gmail.com (A.M.R.); jikangf@yahoo.com (J.K.F.). Fax: +86 431 88945942.
† Institute of Theoretical Chemistry, Jilin University.
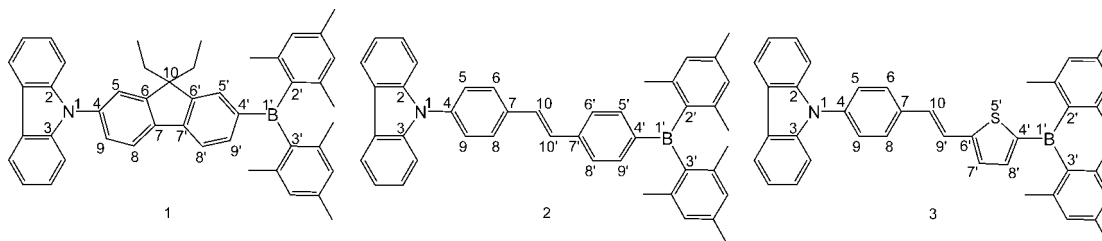‡ College of Chemistry, Jilin University.

Multifunctional Electroluminescent Molecules

J. Phys. Chem. A, Vol. 112, No. 47, 2008 **12173**

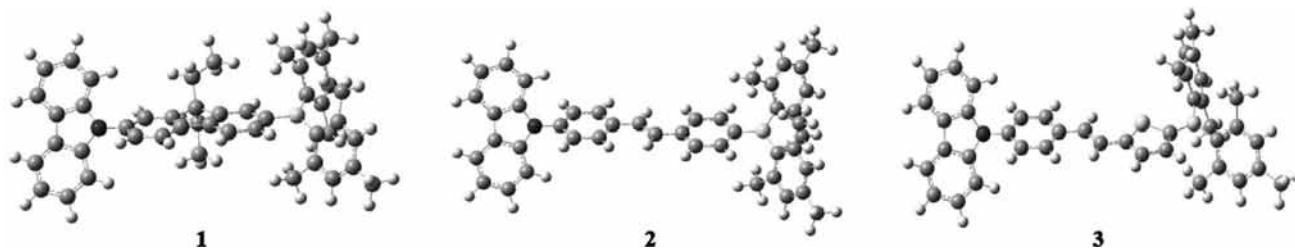**Figure 1.** Sketch map of the studied structures.

Figure 2. The stereograph of optimized compounds **1−3** by DFT//B3LYP/6-31G(d).

TABLE 1: Selected Important Bond Lengths (Ångstroms), Bond Angles (Degrees), and Dihedral Angles (Degrees) of Compounds 1−3 Obtained by B3LYP/6-31G(d) Calculations

	1			2			3		
	neutral	cationic	anionic	neutral	cationic	anionic	neutral	cationic	anionic
$r(1,2)$	1.400	1.411	1.392	1.401	1.413	1.392	1.402	1.415	1.392
$r(1,3)$	1.400	1.410	1.392	1.401	1.413	1.392	1.401	1.414	1.392
$r(1,4)$	1.421	1.400	1.432	1.418	1.395	1.431	1.417	1.393	1.431
$r(1',2')$	1.587	1.578	1.610	1.586	1.575	1.606	1.586	1.573	1.605
$r(1',3')$	1.586	1.575	1.604	1.586	1.575	1.606	1.587	1.570	1.608
$r(1',4')$	1.570	1.586	1.533	1.569	1.586	1.528	1.547	1.575	1.506
$\theta(2,1,4)$	125.8	125.9	125.8	125.8	125.9	126.0	125.9	125.9	125.9
$\theta(2,1,3)$	108.3	108.4	108.1	108.3	108.3	108.2	108.3	108.2	108.2
$\theta(3,1,4)$	125.8	125.7	126.0	125.8	125.8	125.9	125.8	125.9	125.9
$\theta(2',1',4')$	118.4	118.0	119.8	118.8	118.5	120.2	119.2	117.9	121.1
$\theta(2',1',3')$	122.5	123.2	119.6	122.5	123.3	119.7	123.5	125.0	120.6
$\theta(3',1',4')$	119.1	118.8	120.5	118.7	118.2	120.1	117.4	117.1	118.3

compounds were studied by employing TD-DFT and TD-HF methods. TD B3LYP//CIS method is considered to precisely predict the fluorescent spectra of these systems[21−25] (see Supporting Information). The polarizable continuum model (PCM) was used in calculation of the emission spectra in THF. The various properties of these compounds, such as ionization potentials, electron affinities, reorganization energy (λ), and fluorescence lifetime (τ), were derived from the computed results. In addition, compositions of molecular orbitals and overlap populations between molecular fragments were analyzed using the PYMOLYZE program.[26] All DFT calculations were performed using the B3LYP functional and the 6-31G (d) basis set.

3. Results and Discussion

3.1. Geometry Optimization. The sketch maps of the studied compounds are depicted in Figure 1, and the optimized structures of compounds **1**, **2**, and **3** by B3LYP/6-31G(d) are plotted in Figure 2. The selected important bond lengths and bond angles of these compounds in the neutral, cationic, and anionic states obtained by DFT//B3LYP/6-31G(d) calculations are listed in Table 1.

From Figure 1, it can be clearly seen that **1**, **2**, and **3** have the same frame on both sides of the molecules but different π-conjugated bridges in the middle. As shown in Table 1, the angles around both N and B atoms in compounds **1**, **2**, and **3** for $\theta(2,1,4)$, $\theta(2,1,3)$, $\theta(3,1,4)$, $\theta(2',1',4')$, $\theta(2',1',3')$, and

$\theta(3',1',4')$ are very close to each other in the neutral, cationic, and anionic states, respectively. The sums of the angles around both N and B atoms are very close to 360° for compounds **1**, **2**, and **3** in all states. Thus, their geometries must be planar around both N and B atoms. In the neutral state, the bond lengths $r(7,10)$ and $r(7',10')$ of compound **2** are all 1.463 Å. In compound **3**, bond $r(7,10)$ is 1.460 Å, while bond $r(6',9')$ is reduced to 1.445 Å due to the thiophene ring. It is noted that the bond length $r(1',4')$ of compound **3**, which is 1.547 Å, is the shortest B−C bond in the three compounds. This remarkably strengthened B−C bonding, combining with the well conjugated π-bridge, indicates some charge transfer on excitation probably due to the presence of thiophene. The bond lengths in these states were analyzed and found that the bonds $r(1,4)$, $r(1',2')$, and $r(1',3')$ in the neutral state are longer than in the cationic state but shorter than in the anionic state. Whereas, the bonds $r(1',4')$, $r(1,2)$, and $r(1,3)$ in the neutral state are longer than those in the anionic but shorter than those in the cationic state. It indicated that removing an electron will decrease the $r(1,4)$, $r(1',2')$, and $r(1',3')$ antibonding interaction and lead to shorter distances, while accepting an electron will increase the $r(1',4')$, $r(1,2)$, and $r(1,3)$ antibonding interaction and result into much longer distance.

The first excited-state geometries of compounds **1**, **2**, and **3** by CIS/6-31G(d) and corresponding ground structures by HF/6-31G(d) are shown in Table 2. Some of the bond lengths are lengthened, but some are shortened. These differences in the

TABLE 2: Optimized Important Interring Distances (Ångstroms) and Dihedral Angles (Degrees) of Compounds 1−3 with HF/6-31G(d) and CIS/6-31G(d)

	HF			CIS		
	1	2	3	1	2	3
$r(1,2)$	1.387	1.387	1.388	1.397	1.395	1.394
$r(1,3)$	1.387	1.387	1.387	1.396	1.395	1.394
$r(1,4)$	1.420	1.418	1.418	1.396	1.401	1.405
$r(4,5)$	1.390	1.386	1.385	1.409	1.406	1.400
$r(5,6)$	1.382	1.384	1.384	1.365	1.365	1.370
$r(6,7)$	1.393	1.393	1.393	1.433	1.425	1.417
$r(7,8)$	1.386	1.395	1.396	1.424	1.426	1.419
$r(8,9)$	1.385	1.381	1.381	1.363	1.370	1.372
$r(9,4)$	1.390	1.389	1.389	1.417	1.400	1.397
$r(1',2')$	1.599	1.599	1.598	1.606	1.602	1.601
$r(1',3')$	1.599	1.599	1.599	1.603	1.602	1.601
$r(1',4')$	1.582	1.581	1.566	1.559	1.564	1.547
$r(4',5')$	1.403	1.400	1.746	1.428	1.416	1.745
$r(5',6')$	1.381	1.381	1.730	1.362	1.365	1.760
$r(6',7')$	1.396	1.396	1.359	1.441	1.432	1.416
$r(7',8')$	1.385	1.393	1.423	1.426	1.429	1.371
$r(8',9')$	1.384	1.383		1.358	1.361	
$r(9',4')$	1.400	1.397		1.439	1.423	
$r(4',8')$			1.361			1.411
$r(7,10)$		1.477	1.475		1.410	1.419
$r(7',10')$		1.476			1.405	
$r(10,10')$		1.328			1.398	
$r(10,9')$			1.329			1.391
$r(6',9')$			1.462			1.390
$r(7,7')$	1.470			1.397		
$\Phi(6,7,7',6')$	0.43			0.22		
$\Phi(8,7,10,10')$		22.39			0.22	
$\Phi(10,10',8',7')$		20.96			0.15	
$\Phi(8,7,10,9')$			18.86			0.59
$\Phi(5',6',9',10)$			2.31			0.17

bond lengths between the ground (S_0) and singlet excited state (S_1) may be attributed to MO nodal patterns. Because the lowest singlet state corresponds to an excitation from the HOMO to the LUMO in all of the considered compounds, we explore the bond-length variation by analyzing the composition of the HOMO and LUMO. By analysis of Table 2 and Figure 3, it can be seen that the HOMO has nodes across the $r(1,4)$, $r(5,6)$, $r(8,9)$, $r(7,7')$, $r(1',4')$, $r(5',6')$, and $r(8',9')$ bonds in compound 1, $r(1,4)$, $r(5,6)$, $r(8,9)$, $r(7,10)$, $r(1',4')$, $r(5',6')$, $r(8',9')$, and $r(7',10')$ bonds in compound 2, and $r(1,4)$, $r(5,6)$, $r(8,9)$, $r(7,10)$, $r(1',4')$, $r(7',8')$, and $r(6',9')$ bonds in compound 3, but the LUMO is bonding in these above-mentioned regions. Therefore, one can expect contraction of these bonds. The data (Table 2) show that these bonds indeed get to be shortened in the excited state. However, the bond length will increase from the bonding to antibonding. The LUMO has a node across the $r(1,2)$, $r(1,3)$, $r(4,5)$, $r(6,7)$, $r(7,8)$, $r(9,4)$, $r(1',2')$, $r(1',3')$, $r(4',5')$, $r(6',7')$, $r(7',8')$, and $r(9',4')$ bonds in compound 1, $r(1,2)$, $r(1,3)$, $r(4,5)$, $r(6,7)$, $r(7,8)$, $r(9,4)$, $r(1',2')$, $r(1',3')$, $r(4',5')$, $r(6',7')$, $r(7',8')$, $r(9',4')$, and $r(10,10')$ bonds in compound 2, and $r(1,2)$, $r(1,3)$, $r(4,5)$, $r(6,7)$, $r(7,8)$, $r(9,4)$, $r(1',2')$, $r(1',3')$, $r(5',6')$, $r(6',7')$, $r(7',8')$, $r(4',8')$, and $r(10,9')$ bonds in compound 3 while the HOMO is bonding. The data confirm the anticipated elongation of these bonds.

The bridge bonds between two conjugated segments rotate to some extent. The dihedral angle in compounds 1, 2, and 3 decreases from 0.43, 22.39, 20.96, 18.86, and 2.31 to 0.22, 0.22, 0.15, 0.59, and 0.17, respectively. It is obvious that the excited structure has a strong coplanar tendency in these compounds, as the conjugation is much stronger in the excited structure. As a planar structure of compound 1 in both the ground and excited

states, diethylfluorene-based compound has rigidly planar properties. Furthermore, the dipole moments for compounds 1, 2, and 3 by HF/6-31G(d) (B3LYP/6-31G(d)) are 1.89 D (1.29 D), 1.73 D (0.77 D), and 1.84 D (1.03 D), respectively. These can prove that compound 1 with diethylfluorene-based bridge has a better electron push−pull ability upon excitation than others (see Table S1 of Supporting Information). Meanwhile, the main characters of the front orbitals, the change trend of bond lengths, bond angles, and the dipole moments, calculated by HF/6-31G(d), are close to those values, which were estimated by B3LYP/6-31G(d).

3.2. Frontier Molecular Orbitals. It will be useful to confirm the HOMO and the LUMO of the molecules. The relative ordering of the occupied and virtual orbitals provides a reasonable qualitative indication of the excitation properties[27] and of the ability of electron or hole transportation. Since the first dipole-allowed electron transitions, and the strongest electron transitions with largest oscillator strength, usually correspond almost exclusively to the promotion of an electron from HOMO to LUMO (see section 3.3), we have plotted the electronic density contours of the frontier orbitals of compound 1, 2 and 3 by GaussView in Figure 3.

As shown in Figure 3, it is noted that the electronic cloud distribution of HOMO in compounds 1, 2, and 3 localizes at the side of the nitrogen atom, while the one of LUMO localizes at the side of boron atom. The transition from the benzene rings connected with atom N to those connected with atom B is attributed to the electron push−pull effect of substitutes. The nitrogen and boron atoms are the centers of the electron donor and acceptor, respectively. However, the HOMO-3 of compounds 1, 2, and 3 is strongly confined to the two mesityl groups. In the HOMO-1 of compound 3, the contribution comes from the whole molecule.

The HOMO and LUMO energies are experimentally estimated from an empirical formula proposed by Brédas et al. based on the onset of the oxidation and reduction peaks measured by cyclic voltammetry.[28] These properties of the materials are usually estimated by the values of HOMO and LUMO, in accord with the work function values of cathode and anode. The hole-transport material with the smaller negative value of HOMO should lose their electrons more easily, while the electron-transport material with larger negative value of LUMO should accept electrons more easily. The HOMO and LUMO energies were calculated by DFT in this study. The HOMO and LUMO energies of these orbitals in compounds 1, 2, and 3 are listed in Table 3.

From Table 3, it can be seen that the HOMO and LUMO levels for compounds 1, 2, and 3 were found to be −5.28 and −1.82, −5.28 and −2.07, and −5.27 and −2.21 eV, respectively, which match well with the energy levels for Mes$_2$B[p-4,4'-biphenyl-NPh(1-naphthyl)] (BNPB) (ϵ_{HOMO}, −5.30 eV) and (ϵ_{LUMO}, −2.44 eV).[13] According to the results of these compounds, there was no change in HOMO but a gradual decrease of values in LUMO, which lead to the red shift of the spectrum. It can be deduced that the different π-conjugated bridges showed greater influence on the LUMOs than the HOMOs. These compounds are small molecules with similar shapes and molecular weight to BNPB.[13] Therefore, compounds 1, 2, and 3 may act as trifunctional (emitter, electron-transport, and hole-transport) molecular OLEDs.

Generally, the higher the value of HOMO is, the easier creating a hole is. N,N'-Diphenyl-N,N-bis-(1-naphthyl)-1,1-biphenyl-4,4-diamine (NPD) is a well-known hole-transport material. The value of HOMO in BNPB is obvious higher than
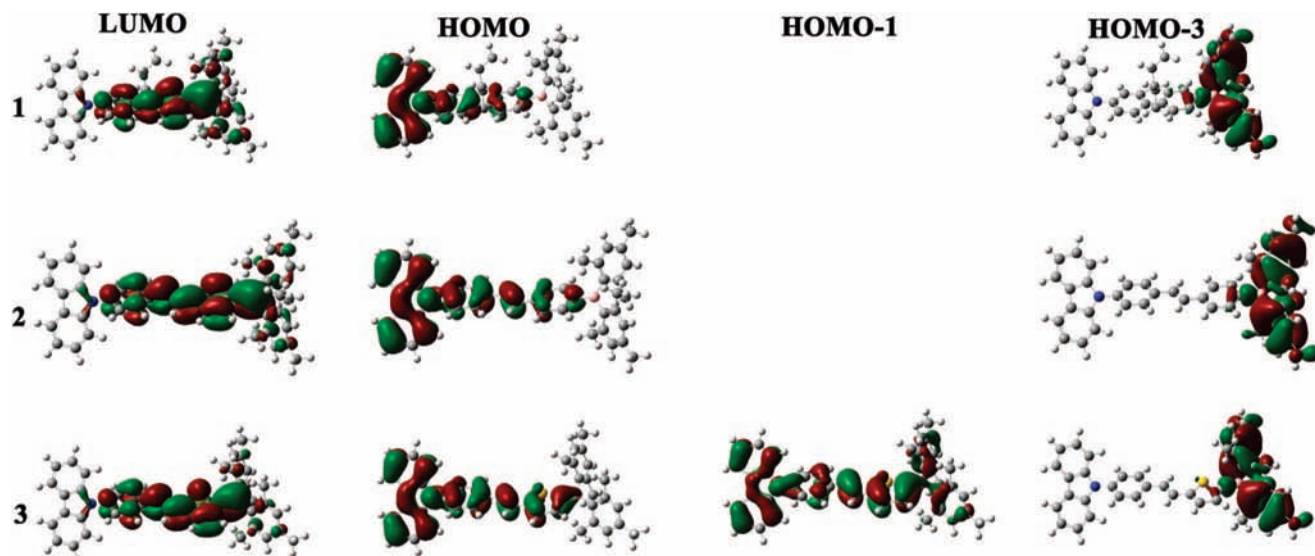
Multifunctional Electroluminescent Molecules

J. Phys. Chem. A, Vol. 112, No. 47, 2008 **12175**

Figure 3. Electronic density contours of the frontier orbitals for compounds **1**−**3**.

TABLE 3: Negative Value of the HOMO (−ϵ_{HOMO}) and LUMO (−ϵ_{LUMO}) Energies, HOMO−LUMO Gaps Calculated by DFT, and the Lowest Excitation Energies Calculted by TD-DFT in eV for Compounds 1−3

	1	2	3
−ϵ_{HOMO}	5.28	5.28	5.27
−ϵ_{LUMO}	1.82	2.07	2.21
Δ_{H-L}	3.46	3.21	3.06
E_g(TD)	3.07	2.87	2.72

TABLE 4: Contribution of Electron Density (%) for Compounds 1−3

	D group		π group		A group	
	HOMO	LUMO	HOMO	LUMO	HOMO	LUMO
1	78.7	1.6	20.2	51.1	1.1	47.4
2	67.6	1.6	31.2	65.9	1.2	32.5
3	58.6	1.6	38.6	71.5	2.8	26.9

that of NPD (−5.5 eV) due to the group of −B(Mes)$_2$, despite the same donors and the π bridges of BNPB and NPD. The HOMO levels of compounds **1**−**3** are almost equal to those of BNPB, showing their good HT ability. Though the LUMO level of compounds **1**−**3** is slightly higher than that of tris(8-hydroxylquinoline)aluminum (Alq$_3$, −3.0 eV), as typical three-coordinate boron compounds; these compounds are still good electron-transport materials due to the availability of the empty p$_\pi$ orbital on the boron center. Again, the LUMO levels of these compounds are close to those of 2-(4-biphenylyl)-5-(4-*tert*-butylphenyl)-1,3,4-oxadiazole (PBD, −2.4 eV), one of the most widely used ET/hole blocking materials.[11,13,29,30] In addition to these above, to shed light on the chemistry activity[31] of the same D and A groups with different π bridges in HOMO and LUMO, the local density of states (LDOS) of compounds **1**, **2**, and **3** has been compared in Table 4. These groups in compound **1** with a diethylfluorene bridge have larger contribution to HOMO and LUMO in comparison to compounds **2** and **3**. This indicates that these groups in compound **1** have better chemistry activity and can effectively carry out intramolecular charge transfer upon exciton. In view of the same substituents on both sides of these molecules, the diethylfluorene unit is a better electron transmitter than the stilbene and styrylthiophene units.

3.3. HOMO−LUMO Gaps and the Lowest Excitation Energies. The energy gaps of compounds **1**, **2**, and **3** are theoretically obtained from the orbital energy differences between the HOMO and LUMO, termed the HOMO−LUMO gaps (Δ_{H-L}).[32,33] But there are three types of band gaps in experiment, namely, optical band gap, electrochemical band gap, and the band gap from photoelectron spectrum. Among these band gaps, the common one is the optical band gap. The optical band gap is obtained from the lowest transition (or excitation) energy from the ground-state to the first dipole-allowed excited state. The first dipole-allowed excited state is the lowest excited singlet state (S$_1$), an electron is promoted from the HOMO to the LUMO under the implicit assumption that the lowest excited singlet state can be described by only one singly excited configuration. In fact, the optical band gap is not the orbital energy difference between the HOMO and LUMO but the energy difference between the S$_0$ state and the S$_1$ state. Only when the excitation to the S$_1$ state corresponds almost exclusively to the promotion of an electron from the HOMO to the LUMO can the optical band gap be approximately equal to the HOMO−LUMO gap in quantity. In this article, the optical band gaps of compounds **1**, **2**, and **3** from the absorption spectra are computed at the TD-DFT level and abbreviated as E_g.

The HOMO−LUMO gaps and lowest singlet excited energies of compounds **1**, **2**, and **3** are listed in Table 3. The HOMO−LUMO energy gaps (Δ_{H-L}) obtained by B3LYP/6-31G(d) are larger than the E_g values from TDDFT//B3LYP/6-31G(d) calculations.[34] It could be ascribed to the neglect of interelectronic interaction upon the single one-electron excitation in estimating Δ_{H-L}. Although there are discrepancies between the computed Δ_{H-L} and E_g, the variation trend is similar. The orders of the energy gaps for Δ_{H-L} and E_g are **1** > **2** > **3**. The absorption and emission spectra of diethylfluorene-based, stilbene-based, and styrylthiophene-based compounds are expected to be gradually red-shifted. As we know, the blue-emitting OLEDs often have a large enough band gap (>3 eV) and a set of matching LUMO/HOMO level to effect the sensitization.[35,36] As the band gaps of diethylfluorene-based compound obtained via the above-mentioned two methods are all higher than 3 eV, diethylfluorene-based compound can be used as emitter in blue OLEDs.

3.4. Ionization Potentials and Electron Affinities. The adequate and balanced transport of both injected electrons and holes is important in optimizing the performance of OLED devices. The ionization potential (IP) and electron affinity (EA) are well-defined properties that can be calculated by DFT to

12176 *J. Phys. Chem. A, Vol. 112, No. 47, 2008*

Zou et al.

TABLE 5: IPs, EAs, Extraction Potentials, and Reorganization Energies for Each Molecule (eV)

	IP(v)	IP(a)	HEP	EA(v)	EA(a)	EEP	λ_{hole}	$\lambda_{\text{electron}}$
1	6.45	6.37	6.27	0.72	0.86	1.00	0.18	0.27
2	6.39	6.30	6.19	0.97	1.14	1.32	0.20	0.35
3	6.35	6.22	6.08	1.07	1.25	1.45	0.27	0.38

estimate the energy barrier for the injection of both holes and electrons into the compounds. Table 5 contains the calculated IPs and EAs, both vertical (v, at the geometry of the neutral molecule) and adiabatic (a, optimized structure for both the neutral and charged molecule), and the extraction potentials (HEP and EEP for the hole and electron, respectively) that refer to the geometry of the ions.[37,38]

One general challenge for the application of small molecules in OLEDs is achievement of high EA molecules and low IP molecules to improve electron and hole injection/transport in electronic devices, respectively. For photoluminescent materials, the lower the IP of the hole-transport layer (HTL), the easier the entrance of holes from ITO to HTL; and the higher the EA of the electron-transport layer (ETL), the easier the entrance of electrons from cathode to ETL. In Table 5, it is shown that the IP(a)s and EA(a)s of **1**, **2**, and **3** are ∼6.37 and 0.86, 6.30 and 1.14, and 6.22 and 1.25 eV, respectively. The change trends of the IPs and EAs for compounds **1**, **2**, and **3** are similar to those of the negative of HOMO and LUMO energies. It has been experimentally proved that BNPB is an good trifunctional molecule.[13,21] As the IPs of compounds **1**, **2**, and **3** are close to that of BNPB (6.08 eV), they can be applied as the HTL materials. By analysis of the values of EAs, compounds **1**, **2**, and **3** are easier to accept an electron than BNPB (0.77 eV),[21] despite of the same acceptor of compounds **1**, **2**, and **3** and BNPB. Therefore compounds **1**, **2**, and **3** exhibit more excellent properties as ETL materials than BNPB due to the presence of various π-conjugated bridges.

As is well-known, organic π-conjugated materials are assumed to transport charge at room temperature via a thermally activated hopping-type mechanism.[34,39,40] In the case of LEDs, the charge transport mechanism can be described as a self-exchange transfer process, for example, an hole-transfer process between adjacent species can be summarized as follows

$$M + M^+ \rightarrow M^+ + M$$
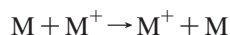
where M represents the neutral species undergoing charge transfer and M^+ the species containing the hole. If the temperature is sufficiently high to treat vibrational modes classically, then the standard Marcus model yields the following expression for the hole (or electron) charge transfer rate,[41−43] (K_{hole}) can be calculated using the following equation, assuming that hole traps are degenerate

$$K_{\text{hole}} = \left(\frac{\pi}{\lambda k_b T}\right)^{1/2} \frac{V^2}{\hbar} \exp\left(-\frac{\lambda}{4 k_b T}\right) \quad (1)$$

where T is the temperature, k_b the Boltzmann constant, λ the reorganization energy due to geometric relaxation accompanying charge transfer, and V the electronic coupling matrix element between the two species. It can be seen from eq 1 that there are two factors λ and V determine the K_{hole}. However, intermolecular (between M and M^+) charge transfer range in noncrystal is rather narrow and V value is very limited; therefore the mobilities of electrons and holes are expected to be dominated by the reorganization energies λ in the exponential term of eq 1 for OLEDs materials.[44,45] The reorganization energy λ (herein the
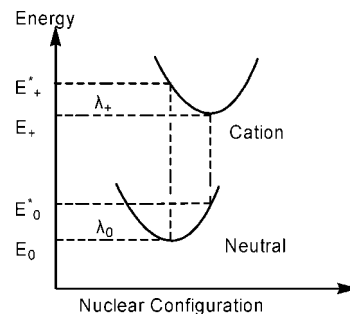
Figure 4. Schematic description of internal reorganization energy for hole transfer.

internal reorganization energy obtained by ignoring any environmental relaxation and changes) for hole transfer can be expressed as follows

$$\lambda_{\text{hole}} = \lambda_0 + \lambda_+ = (E^*_0 - E_0) + (E^*_+ - E_+) \quad (2)$$

As illustrated in Figure 4, E_0 and E_+ represent the energies of the neutral and cation species in their lowest energy geometries, respectively, while E^*_0 and E^*_+ represent the energies of the neutral and cation species with the geometries of the cation and neutral species, respectively. In this way, λ for electron transfer can be expressed as follows

$$\lambda_{\text{electron}} = \lambda_0 + \lambda_- = (E^*_0 - E_0) + (E^*_- - E_-) \quad (3)$$

The calculated λ_{hole} and $\lambda_{\text{electron}}$ values are also listed in Table 5. As emitting layer materials, it needs to achieve the balance between hole injection and electron acceptance. Furthermore, the lower the λ values, the bigger the charge-transport rate. The data (Table 5) show that the λ_{hole} for compounds **1**, **2**, and **3** are all smaller than their respective $\lambda_{\text{electron}}$. It suggests that the hole transfer rate is higher than the electron transfer rate. The λ_{hole} and $\lambda_{\text{electron}}$ of compound **1** are lower than those of compounds **2** and **3**, indicating that diethylfluorene-based compound has a bigger charge-transport rate than the stilbene-based and styrylthiophene-based compounds. Moreover, the difference between the λ_{hole} and $\lambda_{\text{electron}}$ for diethylfluorene-based compound is only 0.09 eV, implying that diethylfluorene-based compound has better equilibrium properties than stilbene-based and styrylthiophene-based compounds. Therefore, the diethylfluorene-based compound is a better emitter with high quantum efficiency. Because the difference between the λ_{hole} and $\lambda_{\text{electron}}$ for compounds **1**, **2**, and **3** are less than 0.15 eV, they can act as the emitter with relatively high light emitting efficiencies. Replacement of benzene with thiophene has no positive effect on charge-transport rate,[15] but it improves the balance between hole-transfer and electron-transfer, which is a greater benefit to increase the produce of the exciton. Thus the effective luminescence is enhanced. As a result, the order of the light-emitting efficiencies of these compounds is **1** > **3** > **2**. Meanwhile, the value of λ both of hole and electron are increased in the order from **1** to **2** and then to **3**. We predict that the Stokes shift have the same order due to the degree of geometric distortion upon excitation.

3.5. Absorption Spectra and Emission Spectra. TDDFT// B3LYP/6-31G(d), TD BHandHLYP/6-31+G(d,p), and TD HF/ 6-31G(d) have been used to study the nature and the energy of absorption and emission spectra of these molecules on the basis of the optimized geometries. However, TD B3LYP is a feasible method compared to other two methods and is widely applied in exploring the calculated spectra (the detailed analysis of the calculated spectra is presented in the Supporting Information).[21−25]

TABLE 6: Absorption Spectra Obtained by TD-DFT Methods for Compounds 1−3 at the B3LYP/6-31G(d) Optimized Geometries

	electronic transitions	λ^{abs}_{max} (nm)	exp^a (nm)	f	excitation energies (eV)	main configurations	
1	$S_0 \rightarrow S_1$	403.6	355	0.41	3.07	HOMO → LUMO	0.69
	$S_0 \rightarrow S_2$	354.7		0.07	3.50	HOMO-3 → LUMO	0.69
2	$S_0 \rightarrow S_1$	431.5	359	0.76	2.87	HOMO → LUMO	0.68
	$S_0 \rightarrow S_2$	375.4		0.06	3.30	HOMO-3 → LUMO	0.68
						HOMO-3 → LUMO+1	0.12
3	$S_0 \rightarrow S_1$	455.7	397	0.82	2.72	HOMO → LUMO	0.67
	$S_0 \rightarrow S_2$	390.9		0.23	3.17	HOMO-1 → LUMO	0.54
						HOMO-3 → LUMO	−0.32
						HOMO-4 → LUMO	0.14
						HOMO-5 → LUMO	0.18
						HOMO-6 → LUMO	0.10

a Measured in THF.[15,16]

**TABLE 7: Calculated Emission Data in Gas and Solvent THF for Compounds 1−3**

	electronic transitions	exp^a (nm)	λ^{em} (nm)	f	excitation energies (eV)	main configurations	
1 gas phase	$S_1 \rightarrow S_0$		429.9	0.75	2.88	HOMO → LUMO	0.67
THF	$S_1 \rightarrow S_0$	435	431.2	0.93	2.88	HOMO → LUMO	0.67
2 gas phase	$S_1 \rightarrow S_0$		473.5	1.14	2.62	HOMO → LUMO	0.65
		464				HOMO-1 → LUMO	0.13
THF	$S_1 \rightarrow S_0$		479.9	1.45	2.58	HOMO → LUMO	0.65
3 gas phase	$S_1 \rightarrow S_0$		497.9	1.04	2.49	HOMO → LUMO	0.63
		484				HOMO-1 → LUMO	0.16
THF	$S_1 \rightarrow S_0$		507.3	1.30	2.44	HOMO → LUMO	0.64

a Measured in THF.[15,16]

In this section, the following discussions are all based on the TD B3LYP method.

The transition energies from absorption spectra, oscillator strengths, and configurations for the most relevant singlet excited states in each molecule are listed in Table 6, accompanied by the experimental results. As shown in Table 6, all the electronic transitions are of the $\pi \rightarrow \pi^*$ type, and the excitation to S_1 state corresponds almost exclusively to the promotion of an electron from the HOMO to the LUMO. The oscillator strengths (f) of the lowest $S_0 \rightarrow S_1$ electronic transition are the largest in these compounds, and meanwhile the increasing oscillator strengths (f) of the lowest $S_0 \rightarrow S_1$ results in the red-shift of the λ^{abs}_{max} of these compounds in the order of compounds **1**, **2**, and **3**. However, two factors may cause deviations of the current the calculated data of these compounds based on the experiment values. One is that the calculation of these compounds was on the basis of isolated gas phase, and the experimental values were measured in the liquid phase involving the environmental influences. Another factor that should be born in mind is that polarization effects and intermolecular packing forces had been neglected in the calculations.

In addition, the influence of solvent THF on the emission spectra of compounds **1**, **2**, and **3** was simulated at the B3LYP/6-31G(d) level by using the PCM. By comparison of the results with the emission wavelengths of these compounds in gas phase (listed in Table 7), it can be seen that the emission peaks with the large oscillator strength are all assigned to $\pi \rightarrow \pi^*$ character arising from S_1, a HOMO → LUMO transition. The coefficient and configurations are nearly identical, but slight red-shifts (1.3−9.4 nm) of emission wavelengths occur; the oscillator strengths increase by 2−31%, and the excitation energy deviations are lower than 0.05 eV. The maximum emission wavelengths of these compounds both in THF and gas phase are all
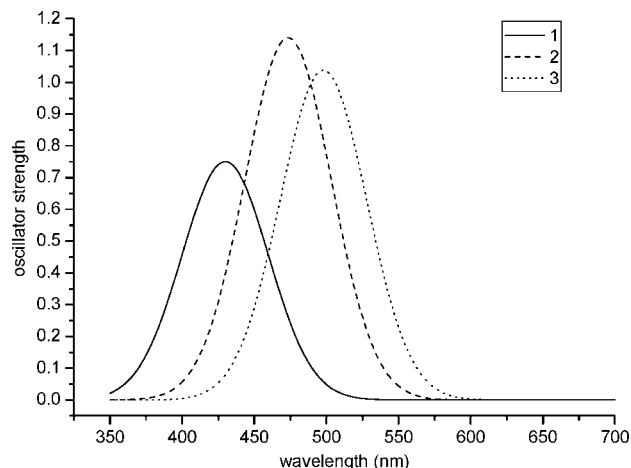
Figure 5. Simulated emission spectra of **1−3** in the gas phase with the calculated data at the TDDFT/B3LYP/6-31G(d) level.

in accordance with the experimental values. The calculated values of the fluorescence wavelength in the gas phase for compounds **1**, **2**, and **3** are located at 429.9, 473.5, and 497.9 nm, respectively (fitted Gaussian type emission curves with the calculated emission data are shown in Figure 5). On the basis of the special emission spectra, we predict that compounds **1**, **2**, and **3** could be used as blue and green light emitting materials. The emission wavelengths for compounds **1**, **2**, and **3** exhibit gradual red shifts, and the Stokes shifts of these compounds in the gas phase are within the range from 26.3 to 42.2 nm. It may be explained that these compounds have large change of the structures in the ground and excited states. Furthermore, the radiative lifetimes have been computed for spontaneous emission by using the Einstein transition probabilities according to the formula (in au)[46,47]

$$\tau = \frac{c^3}{2(E_{Flu})^2 f} \qquad (4)$$

where c is the velocity of light, E_{Flu} is the excitation energy, and f is the oscillator strength (see Table 7). The computed lifetime τ for compounds **1**, **2**, and **3** both in THF and the gas phase are ~3.00 and 3.71, 2.39 and 2.95, and 2.97 and 3.58 ns, respectively; the order of τ both in THF and the gas phase are **1** > **3** > **2**. In the literature, the order of τ: **1** (2.20 ns) > **3** (1.95 ns) > **2** (1.84 ns).[15,16] Obviously, the values of both calculated and experimental have the same sequence in fluorescence lifetimes, and the sequence of fluorescence lifetimes are in accordance with the sequence of the light emitting efficiencies.

4. Conclusions

In this paper, the ground-state and excited-state properties of these compounds are investigated by DFT, TDDFT, and CIS methods. From the above research we conclude that these compounds are excellent candidates for the multifunctional OLED materials. The calculated values of IP and EA show that these compounds can be used as electron-transport and hole-transport materials simultaneously. By analysis of the local density of states and reorganization energy (λ), the diethylfluorene-based compound has higher intra- and intermolecular charge-transfer ability and better equilibrium properties compared to stilbene-based and styrylthiophene-based compounds. Replacing the benzene with thiophene in these compounds has no positive effect on charge-transport rate but enhances the

balance between the hole transfer and electron transfer. With the HOMO−LUMO gaps decreasing, the absorption and emission wavelengths for compounds **1**, **2**, and **3** exhibit gradual red-shifts, and meanwhile the Stokes shifts of these gas-phase compounds, ranging from 26.3 to 42.2 nm, occur due to the large change of the structures in the ground and excited states. The emission wavelengths of these compounds are located at blue and green scope, implying that they can be used as blue and green light emitting materials. Also, the radiative lifetimes have been computed out, which are in accordance with the order of the light emitting efficiencies: **1** > **3** > **2**.

Supporting Information Available: Tables show the Mulliken atomic charges distributions in the ground and excited states for compounds **1**−**3** and analysis of the calculated electronic spectra by TD-B3LYP, TD-BHandHLYP, and TD-HF methods. This material is available free of charge via the Internet at http://pubs.acs.org.

References and Notes

(1) Pope, M.; Kallman, H.; Magnante, P. *J. Chem. Phys.* **1963**, *38*, 2042.

(2) Gurnee, E.; Fernandez, R. U.S. Patent No. 3,172,862, 1965.

(3) Tang, C. W. U.S. Pat. No. 4,356,429, 1995.

(4) Tang, C. W.; Van Slyke, S. A. *Appl. Phys. Lett.* **1987**, *51*, 913.

(5) Friend, R.; Burroughes, J.; Bradley, D. WO Patent, 9,013,148.

(6) Friend, R.; Burroughes, J.; Bradley, D. U.S. Patent No. 5,247,190, 1993.

(7) Peumans, P.; Yakimov, A.; Forrest, S. R. *J. Appl. Phys.* **2003**, *93*, 3693.

(8) Dimitrakopolous, C. D.; Malenfant, P. R. L. *Adv. Mater.* **2002**, *14*, 99.

(9) Kulkarni, A. P.; Tonzola, C. J.; Babel, A.; Jenekhe, S. A. *Chem. Mater.* **2004**, *16*, 4556.

(10) Slinker, J.; Bernards, D.; Houston, P. L.; Abruña, H. D.; Bernhard, S.; Malliaras, G. G. *Chem. Commun.* **2003**, *19*, 2392.

(11) Wong, W. Y.; He, Z.; So, S. K.; Tong, K. L.; Lin, Z. *Organometallics* **2005**, *24*, 4079.

(12) He, Z.; Wong, W. Y.; Yu, X.; Kwork, H. S.; Lin, Z. *Inorg. Chem.* **2006**, *45*, 10922–10937.

(13) Jia, W. L.; Feng, X. D.; Bai, D. R.; Lu, Z. H.; Wang, S.; Vamvounis, G. *Chem. Mater.* **2005**, *17*, 164.

(14) Liu, X. Y.; Bai, D. R.; Wang, S. *Angew. Chem., Int. Ed.* **2006**, *45*, 5475.

(15) Liu, Z. Q.; Fang, Q.; Wang, D.; Cao, D. X.; Xue, G.; Yu, W. T.; Lei, H. *Chem.−Eur. J.* **2003**, *9*, 5074.

(16) Liu, Z. Q.; Cao, D. X.; Fang, Q.; Liu, G. Q.; Xu, G. B. *Acta Chim. Sinica* **2004**, *62*, 2103.

(17) Zhang, H.; Huo, C.; Zhang, J.; Zhang, P.; Tian, W.; Wang, Y. *Chem. Commun.* **2006**, *3*, 281.

(18) Doi, H.; Kinoshita, M.; Okumoto, K.; Shirota, Y. *Chem. Mater.* **2003**, *15*, 1080.

(19) Jia, W. L.; Moran, M. J.; Yuan, Y. Y.; Lu, Z. H.; Wang, S. *J. Mater. Chem.* **2005**, *15*, 3326.

(20) Frisch, M. J.; Trucks, G. W.; Schlegel, H. B.; Scuseria, G. E.; Robb, M. A.; Cheeseman, J. R.; MontgomeryJr., J. A.; Vreven, T.; Kudin, K. N.; Burant, J. C.; Millam, J. M.; Iyengar, S. S.; Tomasi, J.; Barone, V.; Mennucci, B.; Cossi, M.; Scalmani, G.; Rega, N.; Petersson, G. A.; Nakatsuji, H.; Hada, M.; Ehara, M.; Toyota, K.; Fukuda, R.; Hasegawa, J.; Ishida, M.; Nakajima, T.; Honda, Y.; Kitao, O.; Nakai, H.; Klene, M.; Li, X.; Knox, J. E.; Hratchian, H. P.; Cross, J. B.; Adamo, C.; Jaramillo, J.; Gomperts, R.; Stratmann, R. E.; Yazyev, O.; Austin, A. J.; Cammi, R.; Pomelli, C.; Ochterski, J. W.; Ayala, P. Y.; Morokuma, K.; Voth, G. A.; Salvador, P.; Dannenberg, J. J.; Zakrzewski, V. G.; Dapprich, S.; Daniels, A. D.; Strain, M. C.; Farkas, O.; Malick, D. K.; Rabuck, A. D.; Raghavachari, K.; Foresman, J. B.; Ortiz, J. V.; Cui, Q.; Baboul, A. G.; Clifford, S.; Cioslowski, J.; Stefanov, B. B.; Liu, G.; Liashenko, A.; Piskorz, P.; Komaromi, I.; Martin, R. L.; Fox, D. J.; Keith, T.; Ai-Laham, M. A.; Peng, C. Y.; Nanayakkara, A.; Challacombe, M.; Gill, P. M. W.; Johnson, B.; Chen, W.; Wong, M. W.; Gonzalez, C.; Pople, J. A.; *Gaussian 03*, revision B.01; Gaussian Inc.: Pittsburgh, PA, 2003.

(21) Li, X.; Wang, X.; Gao, J.; Yu, X.; Wang, H. *Chem. Phys.* **2006**, *326*, 390.

(22) Yang, L.; Ren, A. M.; Feng, J. K. *J. Org. Chem.* **2005**, *70*, 5987.

(23) Yang, L.; Ren, A. M.; Feng, J. K.; Wang, J. F. *J. Org. Chem.* **2005**, *70*, 3009.

(24) Liu, Y. L.; Feng, J. K.; Ren, A. M. *J. Phys. Chem. A* **2008**, *112*, 3157.

(25) Liu, Y. L.; Feng, J. K.; Ren, A. M. *J. Comput. Chem.* **2007**, *28*, 2500.

(26) Tenderholt, A. PyMOlyze, 2.0; Stanford University: Stanford, CA, 2005.

(27) De Oliveira, M. A.; Duarte, H. A.; Pernaut, J. M.; De Almeida, W. B. *J. Phys. Chem. A* **2000**, *104*, 8256.

(28) Morisaki, Y.; Ishida, T.; Chujo, Y. *Polym. J.* **2003**, *35*, 501.

(29) Kraft, A.; Grimsdale, A. C.; Holmes, A. B. *Angew. Chem., Int. Ed.* **1998**, *37*, 402.

(30) Tamoto, N.; Adachi, C.; Nagai, K. *Chem. Mater.* **1997**, *9*, 1077.

(31) Chen, D. L.; Tian, W. Q.; Feng, J. K.; Sun, C. C. *ChemPhysChem* **2007**, *8*, 1029.

(32) Hay, P. J. *J. Phys. Chem. A* **2002**, *106*, 1634.

(33) Hong, S. Y.; Kim, D. Y.; Kim, C. Y.; Hoffmann, R. *Macromolecules* **2001**, *34*, 6474.

(34) Hutchison, G. R.; Ratner, M. A.; Marks, T. J. *J. Am. Chem. Soc.* **2005**, *127*, 2339.

(35) Hung, L. S.; Chen, C. H. *Mater. Sci. Eng. R* **2002**, *39*, 143.

(36) Tonzola, C. J.; Kulkarni, A. P.; Gifford, A. P.; Kaminsky, W.; Jenekhe, S. A. *Adv. Funct. Mater.* **2007**, *17*, 863.

(37) Curioni, A.; Boero, M.; Andreoni, W. *Chem. Phys. Lett.* **1998**, *294*, 263.

(38) Wang, I.; Botzung-Appert, E.; Stéphan, O.; Ibanez, A.; Baldeck, P. L. *J. Opt. A: Pure Appl. Opt.* **2002**, *4*, S258.

(39) Epstein, A. J.; Lee, W. P.; Prigodin, V. N. *Synth. Met.* **2001**, *117*, 9.

(40) Reedijk, J. A.; Martens, H. C. F.; van Bohemen, S. M. C.; Hilt, O.; Brom, H. B.; Michels, M. A. J. *Synth. Met.* **1999**, *101*, 475.

(41) Marcus, R. A. *J. Chem. Phys.* **1965**, *43*, 679.

(42) Marcus, R. A. *Rev. Mod. Phys.* **1993**, *65*, 599.

(43) Hutchinson, G. R.; Ratner, M. A.; Marks, T. J. *J. Am. Chem. Soc.* **2005**, *127*, 2339.

(44) Nelsen, S. F.; Trieber, D. A.; Ismagilov, R. F.; Teki, Y. *J. Am. Chem. Soc.* **2001**, *123*, 5684.

(45) Nelsen, S. F.; Blomgren, F. *J. Org. Chem.* **2001**, *66*, 6551.

(46) Litani-Barzilai, I.; Bulatov, V.; Gridin, V. V.; Schechter, I. *Anal. Chim. Acta* **2004**, *501*, 151.

(47) Lukeš, V.; Aquino, A.; Lischka, H. *J. Phys. Chem. A* **2005**, *109*, 10232.